

Main flow oriented vorticity noise experiments

Hirschberg, Lionel; Bake, Friedrich; Knobloch, Karsten; Hulshoff, Seven J.

Publication date

2022

Document Version

Final published version

Published in

Internoise 2022 - 51st International Congress and Exposition on Noise Control Engineering

Citation (APA)

Hirschberg, L., Bake, F., Knobloch, K., & Hulshoff, S. J. (2022). Main flow oriented vorticity noise experiments. In *Internoise 2022 - 51st International Congress and Exposition on Noise Control Engineering* (Internoise 2022 - 51st International Congress and Exposition on Noise Control Engineering). the Institute of Noise Control Engineering of the USA, Inc..

Important note

To cite this publication, please use the final published version (if applicable).
Please check the document version above.

Copyright

Other than for strictly personal use, it is not permitted to download, forward or distribute the text or part of it, without the consent of the author(s) and/or copyright holder(s), unless the work is under an open content license such as Creative Commons.

Takedown policy

Please contact us and provide details if you believe this document breaches copyrights.
We will remove access to the work immediately and investigate your claim.



Main flow oriented vorticity noise experiments

Lionel Hirschberg
Imperial College London
Department of Mechanical Engineering, London SW7 2AZ, UK

Friedrich Bake
Bundesanstalt für Materialforschung und -prüfung (BAM)
Unter den Eichen 87, 12205 Berlin, Germany

Karsten Knobloch
Deutsches Zentrum für Luft- und Raumfahrt e.V. (DLR)
Mueller-Breslau-Straße 8, 10623 Berlin, Germany

Seven J. Hulshoff
Delft University of Technology
Faculty of Aerospace Engineering, Kluyverweg 1, 2629HS

Abstract

Entropy inhomogeneities and vorticity spots induce so-called indirect combustion noise when passing through a choked nozzle; referred to as entropy noise and vorticity noise, respectively. We note that vorticity noise depends on the orientation of the vorticity; viz., oriented normal or parallel to the axial main flow. An experimental investigation of parallel component vorticity noise is presented. In the experiment a time-dependent swirling flow was induced by unsteady tangential injection in the pipe upstream of a choked convergent-divergent nozzle. As the resulting swirling flow passes through the nozzle, the axial stretching of the fluid caused an increase in rotation energy. The steady energy conservation in an isentropic flow implies a Mach number higher than unity at the throat and an associated reduction of density. Ergo, the critical mass-flow rate (for fixed reservoir pressure and temperature) decreases quadratically with increasing swirl intensity. The acoustic waves radiated downstream of the nozzle are due to the change in the mass flow through the nozzle. These are a direct measure for this mass-flow modulation. Using a semi-empirical model, this sound production mechanism is demonstrated to be quasi steady. This contradicts the bare assertion found in the literature that sound is produced by the acceleration of vorticity or “vorticity waves.”

1 Introduction

Engineering systems employing turbulent combustion usually have high levels of noise production, due both to direct and indirect combustion-noise sources. Direct sources, due to unsteady gas expansion in flames, have been widely studied [1–3]. Indirect sources include entropy noise and vorticity noise. In particular, both entropy spots and vortices produce sound waves as they exit the combustion chamber through a nozzle or turbine. Some of these sound waves are radiated into the environment, and some are radiated into the combustion chamber. The latter can produce new entropy spots and vortices, which in turn produce new sound waves as they exit the combustion chamber. Under unfavorable circumstances, this results in a feedback loop which promotes combustion instability. Thermoacoustic combustion-chamber instabilities driven by indirect-combustion noise are a potential issue in aeroengines and electrical-power generation turbines [2, 3]; and are a well-known problem in large solid rocket motors [4–9].

In order to cultivate fundamental understanding of complex phenomena such as indirect-combustion noise, it is standard practice to design experiments in which only one effect is dominant [6, 10–16]. A

good example of this are the cold-gas — viz. without combustion — scale experiments of self-sustained pressure pulsations in solid rocket motors reported by Anthoine et al. [6]. Indeed, these demonstrated the importance of the integrated nozzle’s nozzle-cavity volume on indirect noise produced by essentially nonlinear azimuthal-vortex-nozzle interaction. Another example is Bake’s et al. [10] canonical entropy-noise experiment. Moreover, the practice of studying indirect-noise sources in isolation has also been successfully used for the development of analytical and numerical indirect-combustion noise models [17–19].

Of the two indirect-combustion noise sources, entropy noise has been the most widely studied, as evidenced by the high number of citations of two seminal articles by Marble & Candel [17] and Ffowcs Williams & Howe [18]. Vorticity noise, in contrast, has received far less attention.

Kings and Bake [11, 12] performed a series of unique experiments with the aim of advancing the fundamental understating of vorticity noise using a so-called “*Vorticity Wave Generator*.” In their experiment a strong swirl was introduced upstream from a choked convergent-divergent nozzle by means of unsteady tangential injection. This swirl convected downstream where it interacted with the choked nozzle producing an acoustic response recorded in the microphone section downstream from the nozzle. Besides performing acoustic measurements, Kings [12] did extensive hot-wire measurements of the upstream flow for a fixed tangential injection condition. These measurements provided evidence of the swirling nature of the upstream-generated structure created by means of unsteady tangential injection. Moreover, they showed that the swirl changes over time — starting as a thin wall-bounded jet and evolving to a solid-body like rotation.

Kings and Bake [11] hypothesized that sound production in their experiments was due to the “*acceleration of artificial vorticity waves*” through the nozzle. However, subsequent analysis of Kings and Bake’s data by Hirschberg et al. [20, 21] and fresh experiments with an improved experimental setup [13, 16] showed that in Kings and Bake’s [11, 12] experiment the sound production mechanism is the change in axial mass-flow rate as the upstream generated swirl structure is ingested or evacuated by the nozzle [21, 13, 16]. Furthermore, Hirschberg et al. [20] showed — for this particular experiment — that entropy noise and normal shock contributions to the downstream recorded acoustic response are negligible. This led Hirschberg et al. [13, 16] to note that: when it comes to vorticity noise, one should distinguish between sound produced by vorticity oriented normal to the main flow (e.g. the azimuthal-vortex-nozzle interaction in the experiment of Anthoine et al. [6]), and that produced by vorticity oriented parallel to the main flow (axial vorticity) [21, 13]. The latter is expected to be an issue in hybrid-rocket engines [22, 23], gas turbines, and aeroengines, in which combustion is normally swirl stabilised. In these systems, a significant permanent axial vorticity component is present, the perturbations of which are a potential source of sound when interacting with the combustion chamber exit.

The setup used by Kings and Bake [11] had two major shortcomings [21, 13]:

1. The acoustic signal recorded downstream from the nozzle was obscured by acoustic reflections at the downstream open-pipe termination of the setup.
2. The tangentially-injected mass-flow rate was undetermined.

Therefore, Hirschberg et al. [16] made the following improvements to the experimental setup:

1. The elongation of the downstream pipe section to allow the measurement of an anechoic signal of ca. 140 ms. This made the measurement of the acoustic response due to swirl-nozzle or entropy-swirl-nozzle interaction possible.
2. The addition of an unsteady tangential-injection reservoir of known volume, $V_{inj} = 2.8 \times 10^{-3} \text{ m}^3$. Through a calibration procedure — described in Refs. [13, 16] — the injection-reservoir pressure p_{inj} was then related to the unsteady upstream-injected mass-flow rate \dot{m}_{inj} .

Hirschberg et al. [16] used the improved experimental setup to perform fresh experiments. The downstream acoustic response due to swirl-nozzle interaction was found to scale with the square of the

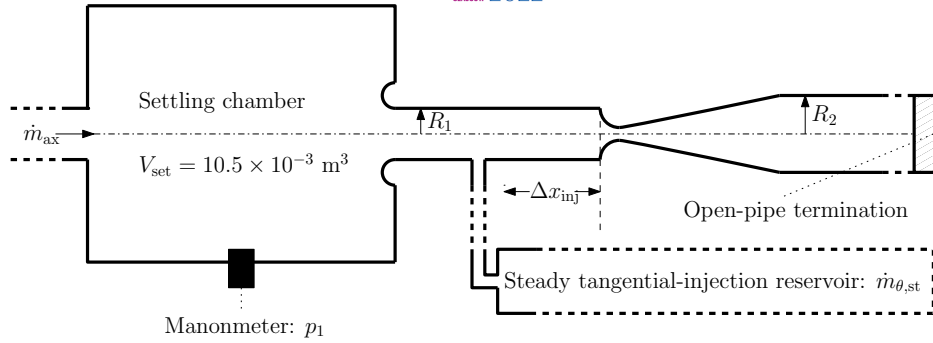


Figure 1: Steady-state measurement setup for the swirl-nozzle interaction experiments.

unsteady-injected tangential mass-flow rate. Hirschberg et al. [16] found that the ingestion and evacuation of the swirl by the choked nozzle produced different amplitudes of the downstream acoustic response. This was attributed to the difference in the swirl at the start (wall-bounded jet) and end (solid-body rotation) of the injection event. Hirschberg et al. [16] developed an empirical quasi-steady model from steady-flow measurements. Their quasi-steady model provided good predictions for the amplitude of the downstream acoustic signal due to the evacuation of swirl. In contrast, it only provided an order-of-magnitude prediction for the amplitude due to swirl ingestion. However, Hirschberg's et al. [16] experiments and analysis showed that — at least in first-order approximation — the acoustic response amplitude can be described by a quasi-steady model [16]; and that the acceleration of vorticity does not play a leading-order role in its determination. Please note that the quadratic response to the swirl magnitude implies that a linear theory will not predict any indirect noise production due to a small swirl perturbation in the absence of a permanent swirl.

In §4, a novel and more apt approach to develop the empirical quasi-steady model is presented. Indeed, the approach presented in §4 is significantly more elegant and effective than the “primitive” method presented in Ref. [16]. Moreover, hitherto unreported acoustic measurements are presented in §3. A brief description of the experimental setups is provided in §2.

2 Description of experimental setups

2.1 Steady-state measurements setup

In Figure 1, a sketch of the setup used to perform steady-state flow measurements is shown. The setup was used to establish a steady-swirl component on a steady axial flow. A Bronckhorst F-203AV linear resistance flow controller was used to set the tangential-injection flow rate, $\dot{m}_{\theta,st}$, through an injection port. In all experiments the total mass-flow rate was kept constant at $1.194 \times 10^{-2} \text{ kg} \cdot \text{s}^{-1}$; viz., $\dot{m}_{tot} = \dot{m}_{\theta,st} + \dot{m}_{ax} = 1.194 \times 10^{-2} \text{ kg} \cdot \text{s}^{-1}$. I.e., whenever e.g. $\dot{m}_{\theta,st,r}$ was varied; \dot{m}_{ax} was varied such that \dot{m}_{tot} remained $1.194 \times 10^{-2} \text{ kg} \cdot \text{s}^{-1}$.

To ensure that a steady state was reached, every time the combination of mass-flow rates was varied, a period of five minutes was allowed to elapse before pressure measurements were carried out. The relative pressure in the settling chamber, $p_1 - p_{atm}$, was measured by means of a MKS Baratron 220D-26159 (1000mBar) manometer. The atmospheric pressure p_{atm} was determined by means of a Wuntronic GmbH temperature/air-humidity/atmospheric pressure transmitter Model T7510.

2.2 Acoustic measurements setup

In Figure 2(a) a sketch of the acoustic-measurement setup is shown. A stationary non-swirling axial base flow, from left to right in Figure 2(a), was created by imposing a mass-flow rate of $\dot{m}_{ax} = 43.0 \text{ kg} \cdot \text{h}^{-1} = 1.194 \times 10^{-2} \text{ kg} \cdot \text{s}^{-1}$ in the settling chamber. This was done using a Bronckhorst F-203AV linear resistance flow controller, connected to a compressed-air supply outlet at $13 \times 10^5 \text{ Pa}$ absolute. At

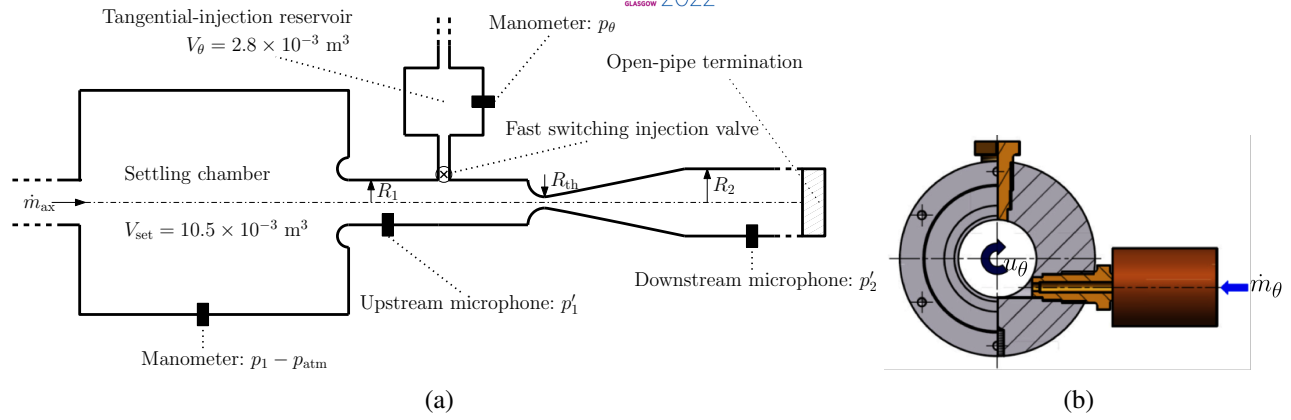


Figure 2: (a) Sketch of the acoustic measurement setup for the swirl-nozzle interaction experiments. Figure is an altered version of Figure 1 in Ref. [16]
 (b) Unsteady tangential-injection system.

$\dot{m}_{\text{ax}} = 1.194 \times 10^{-2} \text{ kg} \cdot \text{s}^{-1}$, choked nozzle conditions were obtained with an upstream reservoir pressure $p_1 = 1.12 \times 10^5 \text{ Pa}$. This imposed an upstream nominal nozzle inlet Mach number of $M_1 = 3.67 \times 10^{-2}$. The reservoir pressure p_1 in the reservoir V_{set} was measured relative to the atmospheric pressure p_{atm} by means of a MKS Baratron 220D-26159 1000 mBar manometer. p_1 is, within the measurement precision, also the steady pressure in the upstream pipe connecting the reservoir to the nozzle inlet. The pressure p_2 in the section downstream from the nozzle was atmospheric p_{atm} and the Mach number was $M_2 = 2.27 \times 10^{-2}$.

The upstream part of the setup (photograph shown in Figure 3) consisted of a settling chamber ($V_{\text{set}} = 10.5 \times 10^{-3} \text{ m}^3$) with a bell-mouth inlet to a tube section (Figure 2(a)). This 220 mm long tube section had a $R_1 = 15 \text{ mm}$ radius. A single tangential-injection port module (Figure 2(b)) was connected to the downstream end of the aforementioned tube section. The injection port module was composed of a 70 mm long upstream pipe section with a radius of $R_1 = 15 \text{ mm}$. At a distance of 266 mm upstream from the nozzle inlet a GRAS 40BP 1/4" ext. polarized pressure microphone was mounted flush in the tube walls. The microphone was calibrated using a Brüel & Kjaer model 4228 pistonphone with $|p'_{\text{ref}}| = 123.92 \text{ dB}$ and $f_{\text{ref}} = 251.2 \text{ Hz}$. This microphone was used to monitor the unsteady pressure rise due to tangential injection [16]. The corresponding acoustic signal p'_1 was recorded using an OROS OR-36 12-channel analyzer with NVGate data acquisition system software, at a sampling frequency of $f_s = 16384 \text{ Hz}$.

Unsteady tangential injection of air into the stationary axial base flow was performed through a port machined in the middle of the module, which had a small converging nozzle of outlet radius of $R_{\theta} = 1.25 \text{ mm}$. Air injection was performed using a fast-switching valve for a variable duration of τ_{θ} . This was repeated every 3 s 100 times. The valve was connected to the converging injection nozzle of diameter $2R_{\theta}$ through a 37 mm long tube with a 4 mm inner diameter. The injection valve was connected to a $V_{\theta} = 2.8 \times 10^{-3} \text{ m}^3$ injection reservoir, by means of a 150 mm long plastic hose with an inner diameter of 12 mm. The injection reservoir was put under a pressure p_{θ} , by means of a compressed-air supply system, connected to the reservoir through a 3.5 m long 12 mm inner diameter hose. p_{θ} was set by means of a valve with a mechanical dial. The dial values were calibrated a posteriori using a NetScanner™ System Model 9116 manometer.

Design details of the injection valve are reported by Neuhaus and Rohle [24], and how it was operated by Kings and Bake [11]. The nominal opening and closing times of the valve were reported by the manufacturer to be 2.5 ms [24]. However, the analysis of acoustic measurements in Ref. [13, 16] showed

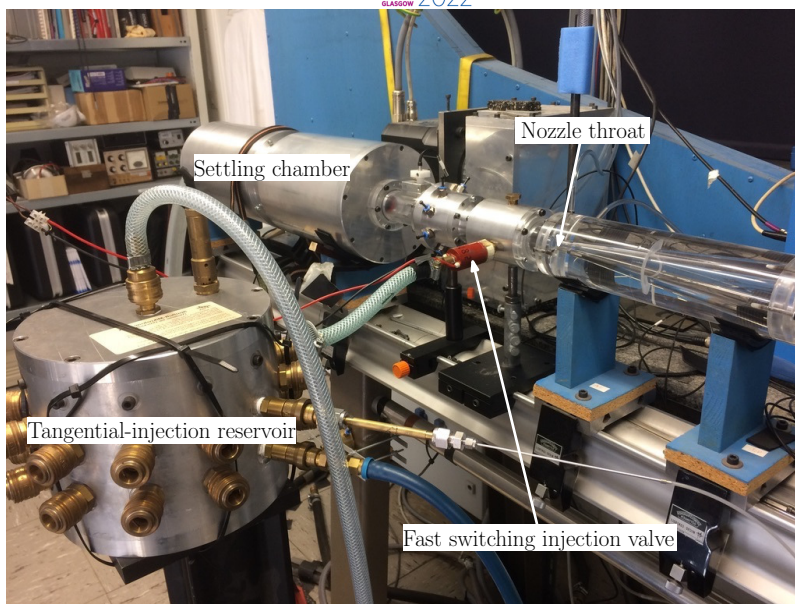


Figure 3: Photograph of the upstream — of the nozzle throat — part of the acoustic-measurement setup including the tangential injection valve and the downstream diverging section of the nozzle.

that in practice, the valve-opening time is smaller. The reported 2.5 ms correspond to the delay between the electrical trigger signal and the injection valve actually opening. Analysis of mass-flow rate calibration measurements reported in Ref. [13], showed that the effective radius of the choked valve was 0.948 mm. In Ref. [16], it was shown that for $p_\theta > 2.5$ bar, the valve was choked and the mass-flow rate was independent of the injection nozzle diameter $2R_\theta$. The data reported here was obtained with choked injection valve conditions.

The tangential injection module was followed downstream by a 50 mm long uniform tube of radius $R_1 = 15$ mm. This tube was connected to a converging-diverging nozzle with throat radius $R_{th} = 3.25$ mm (cross-sectional surface contraction ratio 1/16). The distance between the tangential-injection port and the nozzle inlet was 85 mm. Downstream from the conical divergent part of nozzle (itself 250 mm long) was a uniform tube with a radius of 20 mm and a length of 1020 mm referred to as the “microphone section.”

A GRAS 40BP 1/4" ext. polarized pressure microphone was mounted flush in its walls, calibrated just like the upstream microphone, at a distance 1150 mm from the nozzle throat. This microphone was used to detect pressure waves generated by swirl-nozzle interaction. The corresponding acoustic signal p'_2 was recorded using the same OROS analyzer used to record p'_1 .

The 1020 mm long microphone section was connected downstream to a 24 m long flexible tube of radius $R_2 = 20$ mm. This is a significant improvement, as it prolonged the back-and-forth travel time of acoustic waves from the microphone to the downstream open-pipe termination. This enabled the measurement of the acoustic signal p'_2 due to unsteady swirl-nozzle interaction at the downstream microphone, without the influence of any acoustic reflections for a period of 140 ms. Note that the effective observation time for a constant signal was restricted by the limited low-frequency response of the microphone to about 20 ms [16]. For longer times the microphone signal for a constant pressure decreases rapidly. According to the specifications of the microphone, the deviation in measured amplitude for a harmonic signal of 10 Hz is 1 dB. This corresponds to a 12% deviation in amplitude after 25 ms for a signal increasing linearly with time. That said, the recorded signals are sufficient to perform quantitative analysis of the rapid decrease and increase $\Delta p'_2$ in pressure observed upon ingestion and evacuation of swirl.

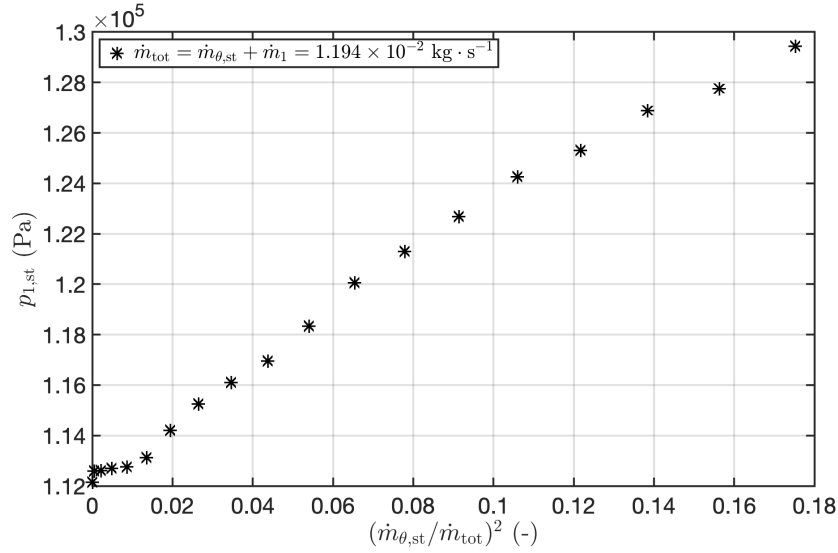


Figure 4: The measured steady upstream-reservoir pressure, $p_{1,st}$, as a function of $(\dot{m}_{\theta,st}/\dot{m}_{tot})^2$. Figure is an altered version of Fig. 5 in Ref. [25] (under review).

3 Results

3.1 Steady-state measurements

In Figure 4, the measured steady upstream-reservoir pressure, $p_{1,st}$, is shown as a function of $(\dot{m}_{\theta,st}/\dot{m}_{tot})^2$ (the steady tangential mass-flow rate divided by the fixed total mass-flow rate squared).

These measurements will be used to inform the empirical quasi-steady model — derived in §4. It will be compared to downstream acoustic response measurements in §4.2.

3.2 Acoustics measurements

In Figure 5, a typical upstream recorded acoustic signal, p'_1 , is shown as a function of time, t . The results were obtained with a trigger-pulse width for tangential injection, τ_{igr} of 10 ms, and a tangential injection mass-flow rate $\dot{m}_{\theta} = 2.78 \times 10^{-3} \text{ kg} \cdot \text{s}^{-1}$. The finely dotted line is the unfiltered signal obtained after performing the phase-averaging procedure — detailed in Ref. [11] — of the 100 consecutive measurements. The thick black line is the moving-averaged filtered (cut-off frequency $f_c = 234.06 \text{ Hz}$) value of this signal.

The signals in Figure 5 are compared to

$$\Delta p'_{1,inj} = \frac{c_1^2 \dot{m}_{\theta}}{V_{set}} (t - t_{open}) \quad (1)$$

where c_1 is the upstream sound speed, \dot{m}_{θ} the tangentially injected mass-flow rate, V_{set} the settling chamber volume, $t_{open} = 2.5 \text{ ms}$. This is a model — the derivation can be found Refs. [13, 16] — for the adiabatic and uniform compression of the air in the upstream reservoir due to the impulsive tangential air injection. The predicted linear increase is shown as a thick dotted line.

In dimensionless form Equation 1, becomes

$$\frac{\Delta p'_{1,inj}}{p_1} = \frac{\gamma \dot{m}_{\theta}}{\rho_1 V_{set}} (t - t_{open}) \equiv \frac{t - t_{open}}{\tau_1} \quad (2)$$

where $\gamma p_1 = \rho_1 c_1^2$ — with $\gamma \equiv c_p/c_v = 1.4$ the heat capacity ratio for air — was used. One observes that first factor in Equation 2 is the inverse of a time constant; viz.

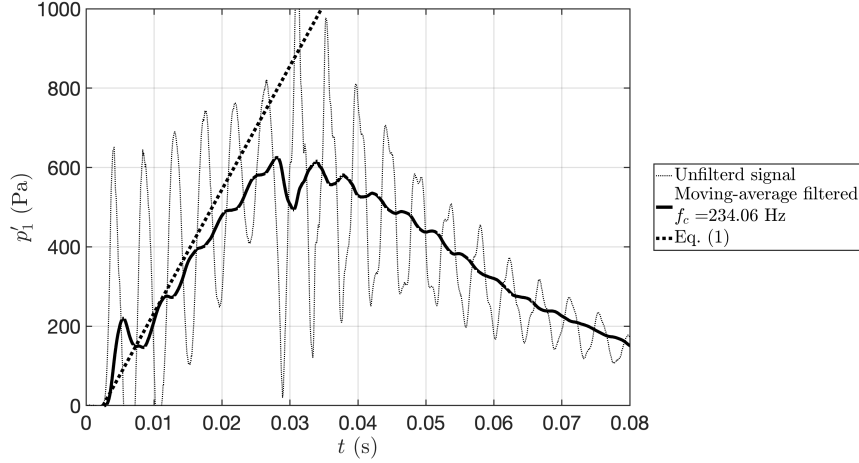


Figure 5: Upstream acoustic response measurement compared to Equation 1. These results were obtained with $\tau_{\text{tgr}} = 10$ ms and $\dot{m}_\theta = 2.78 \times 10^{-3}$ kg \cdot s $^{-1}$.

$$\tau_1 \equiv \frac{\rho_1 V_{\text{set}}}{\gamma \dot{m}_\theta} \simeq 4 \text{ s} \quad (3)$$

This time constant is a measure of the time it takes for the upstream reservoir conditions to adapt in order to evacuate the additional mass injected tangentially, to reach a steady flow. Thus, say one measures $\Delta t_{\text{msr}} = 30$ ms, one has $\Delta t_{\text{msr}}/\tau_1 \simeq 0.01$; viz., the increase in reservoir pressure is not sufficient enough to significantly increase the mass flow through the nozzle. This is exacerbated by the reduction of critical mass-flow rate due to the presence of swirl in the nozzle. Ergo, at least part of the tangentially injected mass-flow will have to go upstream to the reservoir.

In Figure 6, a typical measurement — obtained using the same conditions as for Figure 5 — of the downstream acoustic signal, p'_2 , is shown as a function of time, t . As was the case for p'_1 , the finely dotted line is the unfiltered signal obtained after performing the phase-averaging procedure of the 100 consecutive measurements; the thick black line is the moving-averaged filtered value of this signal. Moreover, the acoustic pulses due to the valve opening and closing are indicated. The acoustic response due to the ingestion and evacuation, $\Delta p'_{2,\text{ingestion}}$ and $p'_{2,\text{evacuation}}$, are highlighted as well. One notices that $|p'_{2,\text{ingestion}}| < |p'_{2,\text{evacuation}}|$, this will be discussed in §4.2.

4 Empirical quasi-steady model

4.1 Derivation of the empirical quasi-steady model

One uses — as was done in Ref. [16] — a simple acoustic model for the downstream acoustic response :

$$\Delta p'_2 = \frac{c_2}{\pi R_2^2} \Delta \dot{m}_{\text{th}} \quad (4)$$

where c_2 is sound speed in the downstream section, πR_2^2 the cross-sectional area of the downstream pipe. $\Delta \dot{m}_{\text{th}}$ is the axial mass-flow rate change through the nozzle throat due to swirl ingestion and evacuation, respectively. One notes that

$$\Delta \dot{m}_{\text{th}} = \begin{cases} < 0 \text{ upon swirl ingestion} \\ > 0 \text{ upon swirl evacuation} \end{cases} \quad (5)$$

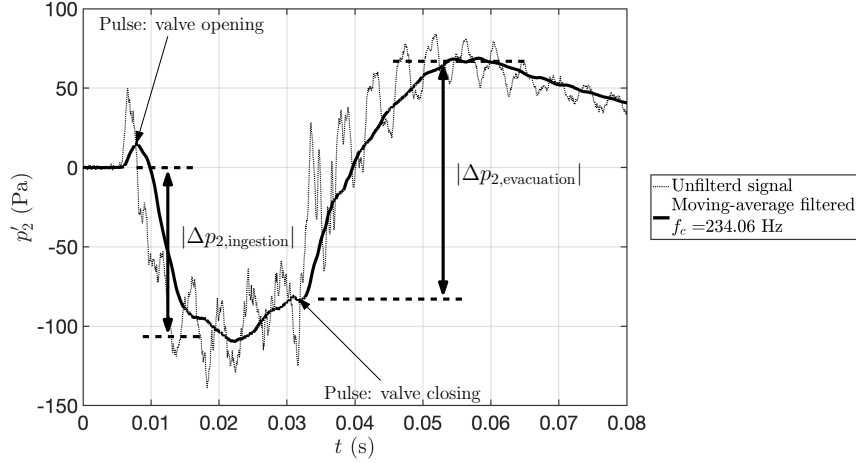


Figure 6: Example of a downstream acoustic response measurement due to swirl ingestion and evacuation. These results were obtained with $\tau_{tgr} = 10$ ms and $\dot{m}_\theta = 2.78 \times 10^{-3} \text{ kg} \cdot \text{s}^{-1}$.

as was established in Refs. [21, 13, 16]. In what follows a novel derivation for an empirical quasi-steady model (QSM) for $\Delta \dot{m}_{th}$ is provided.

\dot{m}_{th} is taken to be a function of the upstream reservoir pressure p_1 and the unsteady tangential injection mass-flow rate squared \dot{m}_θ^2 , viz.:

$$\dot{m}_{th} = \dot{m}_{th}(p_1, \dot{m}_\theta^2) \quad (6)$$

Taking the total differential of Equation 6, one finds

$$\Delta \dot{m}_{th} = \left(\frac{\partial \dot{m}_{th}}{\partial p_1} \right)_{\dot{m}_\theta^2} \Delta p_1 + \left(\frac{\partial \dot{m}_{th}}{\partial \dot{m}_\theta^2} \right)_{p_1} \Delta \dot{m}_\theta^2 \quad (7)$$

One notes that for the steady-state experiments the condition

$$\Delta \dot{m}_{th,st} = 0 \quad (8)$$

was imposed ($\dot{m}_{th} = \dot{m}_{ax} + \dot{m}_\theta = \text{constant}$). In which case Equation 7 reduces to

$$\left(\frac{\partial \dot{m}_{th,st}}{\partial \dot{m}_\theta^2} \right)_{p_1} \Delta \dot{m}_{\theta,st}^2 = - \left(\frac{\partial \dot{m}_{th,st}}{\partial p_{1,st}} \right)_{\dot{m}_\theta^2} \Delta p_{1,st} \quad (9)$$

The short impulsive tangential mass-flow injection \dot{m}_θ leads to an increase of reservoir pressure Δp_1 much smaller than the increase in steady reservoir pressure $\Delta p_{1,st}$ needed to increase the steady mass flow through the nozzle by the same amount \dot{m}_θ . As, $\Delta p_1 / \Delta p_{1,st} \approx 1/20 \ll 1$ (Figure 5) the Equation 7 simplifies to:

$$\Delta \dot{m}_{th} \approx \left(\frac{\partial \dot{m}_{th}}{\partial \dot{m}_\theta^2} \right) \Delta \dot{m}_\theta^2 \quad (10)$$

Using Equation 9 one finds

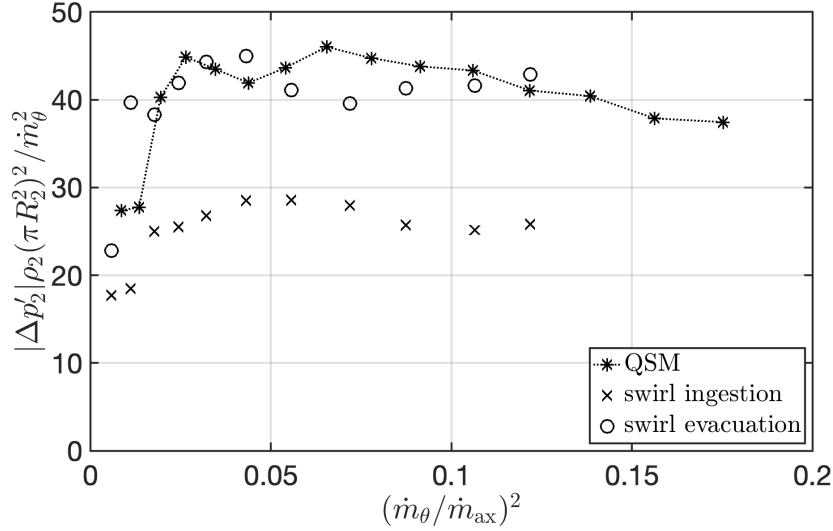


Figure 7: Comparison of the QSM to $\Delta p'_2$ due to swirl ingestion and evacuation. Figure is an altered version of Fig. 7 in Ref. [25] (under review).

$$\Delta \dot{m}_{\text{th,QSM}} = - \left(\frac{\partial \dot{m}_{\text{th,st}}}{\partial p_{1,\text{st}}} \right)_{\dot{m}_\theta^2} \Delta p_{1,\text{st}} \quad (11)$$

where the subscript QSM stands for empirical quasi-steady model. For the partial differential factor in Equation 11, we use

$$- \left(\frac{\partial \dot{m}_{\text{th,st}}}{\partial p_{1,\text{st}}} \right)_{\dot{m}_\theta^2} = - \frac{\pi R_{\text{th}}^2}{c_1} \left(\frac{2}{\gamma + 1} \right)^{\frac{\gamma+1}{2(\gamma-1)}} \quad (12)$$

where c_1 is the upstream sound speed, πR_{th}^2 is cross-sectional surface area at the nozzle throat, and $\gamma \equiv c_p/c_v = 1.4$ is the heat capacity ratio of dry air. This factor was taken from the classical steady quasi-one-dimensional critical mass-flow rate relation for a swirl-free nozzle flow; viz. [26]:

$$\dot{m}_{\text{th}}^* = p_1 \frac{\pi R_{\text{th}}^2}{c_1} \left(\frac{2}{\gamma + 1} \right)^{\frac{\gamma+1}{2(\gamma-1)}} \quad (13)$$

The second factor in Equation 10, $\Delta p_{1,\text{st}}$, is determined from steady-state measurements (Figure 4).

Using the above, the QSM for the downstream measured acoustic response becomes

$$\Delta p'_{2,\text{QSM}} = -\Delta p_{1,\text{st}} \frac{c_2}{c_1} \left(\frac{R_{\text{th}}}{R_2} \right)^2 \left(\frac{2}{\gamma + 1} \right)^{\frac{\gamma+1}{2(\gamma-1)}} \quad (14)$$

In §4.2, this QSM (Equation 14) is compared to acoustic measurement of $\Delta p'_2$ due to swirl ingestion and evacuation.

4.2 Comparison with acoustic response data

In Figure 7, the quasi-steady model (QSM; Equation 14) is compared to acoustic measurements of the downstream acoustic response due to swirl ingestion (crosses) and evacuation (circles).

One observes that there is a very good agreement between the QSM and the swirl-evacuation data. However, one should qualify this assertion, as this excellent agreement is actually due to the particular

choice of the injection time. Indeed, as was shown in [16], the ratio of the pressure increase upon evacuation to the prediction of the QSM varies — depending on the injection time — between 0.8 and 1.6. The largest ratios are found when the injection time is of the order of magnitude of the convection time, L_1/U_1 , in the upstream pipe segment joining the reservoir to the nozzle inlet. Moreover, for most swirl-ingestion data the ratio of indirect-noise amplitude to QSM prediction is systematically lower than unity (ca. 0.6). That said, in all cases the QSM predicts the correct order-of-magnitude of the indirect-noise signal due to evacuation of the swirl from the nozzle.

One notes that in §3.2 it was shown that upstream reservoir pressure, p_1 , needs to rise in order for the additional tangentially injected mass-flow rate \dot{m}_θ to be evacuated; this takes time¹. N.b., τ_1 is at least 4 s (it increases with decreasing \dot{m}_θ), while the duration of the tangential injection event is ca. 25 ms. Ergo, the mass flow through the main nozzle will not change much during the tangential injection event. This implies that a part of the tangentially injected fluid will flow upstream towards the reservoir². Due to this back flow, there will be a gradual accumulation of fluid with swirl upstream from the tangential-injection point. This fluid will be evacuated when the tangential injection stops. This explains why the reduction of mass flow due to the initial ingestion of the swirl will have a smaller amplitude than the increase of mass flow due to the evacuation of the swirl at the end of the experiment. Noting that this effect is quadratic in swirl [13, 16], the difference of 40% between the acoustic signal due to ingestion relative to the QSM and the evacuation data is then explained by a difference of 20% in the swirl.

At any rate, these results confirm the quasi-steady nature of sound production in this experiment, which breaks the bare assertion found in the literature; viz., that sound is produced by the acceleration of vorticity or “vorticity waves.” Indeed, here sound is produced by a change in magnitude of the axial vorticity present in the nozzle.

5 Conclusions

For the experiment reported here, sound production due to swirl ingestion and evacuation by a choked nozzle was demonstrated to be quasi steady. This was done using an empirical quasi-steady model (QSM), constructed using steady-state measurement data. The QSM was found to have very good correlation with the data for swirl evacuation. This contradicts the ipse dixit commonly found in the literature; viz., that sound is produced by the acceleration of vorticity or “vorticity waves.” Indeed, the presented results demonstrate that sound is produced by a change in magnitude of the swirl. Furthermore, we note that generally in the literature clarity and progress are hindered by the fact that some publications — treated as authoritative — do not take the vectorial character of vorticity into account. N.b., sound production due to the vorticity component in the direction of the main flow (axial) discussed here is essentially different from that due to the vorticity normal to the main flow (radial and azimuthal).

Acknowledgements

Lionel Hirschberg carried out the reported measurements while he was the beneficiary of a Deutsches Zentrum für Luft- und Raumfahrt (DLR) - Deutscher Akademischer Austauschdienst (DAAD) postdoctoral fellowship (no. 57424730). The authors thank Angelo Rudolphi, Sebastian Kruck, Oliver Klose, Nico Seiffert and Lech Modrzejewski for the technical support. Analysis and redaction of this text were performed while Lionel Hirschberg was a member of Aimee Morgans’ group at Imperial College London — the authors thank Aimee Morgans for her support. Lionel Hirschberg thanks Catherine Lemaitre and Assa Ashuach for their help.

¹The time scale for this effect, τ_1 , can be estimated using Equation 3.

²Note that such upstream flow of tangentially injected fluid can also occur in a steady flow as reported by Madjenali et al. [23].

References

- [1] W. C. Strahle. On combustion generated noise. *Journal of Fluid Mechanics*, 49(2):399–414, 1971.
- [2] A. P. Dowling and Y. Mahmoudi. Combustion noise. *Proceedings of the Combustion Institute*, 35(1):65–100, 2015.
- [3] A. S. Morgans and I. Duran. Entropy noise: A review of theory, progress and challenges. *International Journal of Spray and Combustion Dynamics*, 8(4):285–298, 2016.
- [4] K. W. Dotson, S. Koshigoe, and K. K. Pace. Vortex shedding in a large solid rocket motor without inhibitors at the segmented interfaces. *Journal of Propulsion and Power*, 13(2):197–206, 1997.
- [5] S. J. Hulshoff, A. Hirschberg, and G. C. J. Hofmans. Sound production of vortex nozzle interactions. *Journal of Fluid Mechanics*, 439:335–352, July 2001.
- [6] J. Anthoine, J.-M. Buchlin, and A. Hirschberg. Effect of nozzle cavity on resonance in large srm: Theoretical modeling. *Journal of Propulsion and Power*, 18(2):304–311, 2002.
- [7] L. Hirschberg, S. J. Hulshoff, J. Collinet, C. Schram, and T. Schuller. Vortex nozzle interaction in solid rocket motors: A scaling law for upstream acoustic response. *Journal of the Acoustical Society of America*, 144(1):EL46–EL51, 2018.
- [8] L. Hirschberg, S. J. Hulshoff, J. Collinet, C. Schram, and T. Schuller. Influence of nozzle cavity on indirect vortex- and entropy-sound production. *AIAA Journal*, 57(7):3100–3103, 2019.
- [9] L. Hirschberg and S. J. Hulshoff. Lumped-element model for vortex-nozzle interaction in solid rocket motors. *AIAA Journal*, 58(7):3241–3244, 2020.
- [10] F. Bake, C. Richter, B. Muhlbauer, N. Kings, I. Rohle, F. Thiele, and B. Noll. The entropy-wave generator (EWG): A reference case on entropy noise. *Journal of Sound and Vibration*, pages 574–598, 2009.
- [11] N. Kings and F. Bake. Indirect combustion noise: noise generation by accelerated vorticity in a nozzle flow. *International Journal of Spray and Combustion Dynamics*, 2(3):253–266, 2010.
- [12] N. Kings. *Indirect combustion noise: Experimental investigation of the vortex sound generation in nozzle flows*. PhD thesis, Technische Universität Berlin, 2015.
- [13] L. Hirschberg, F. Bake, K. Knobloch, and S. J. Hulshoff. Swirl-nozzle interaction experiments: Influence of injection-reservoir pressure and injection time. *AIAA Journal*, 59(7):2806–2810, 2021.
- [14] F. De Domenico, E. Rolland, J. Rodrigues, L. Magri, and S. Hochgreb. Compositional and entropy indirect noise generated in subsonic non-isentropic nozzles. *Journal of Fluid Mechanics*, 910:A5 1–31, 2021.
- [15] M. Wellemann and N. Noiray. Experiments on sound reflection and production by choked nozzle flows subject to acoustic and entropy waves. *Journal of Sound and Vibration*, 492:115799, 2021.
- [16] L. Hirschberg, F. Bake, K. Knobloch, A. Rudolphi, S. Kruck, O. Klose, and S. J. Hulshoff. Swirl-nozzle interaction experiment: Quasi-steady model based analysis. *Experiments in Fluids*, 62(175):1–16, 2021.

- [17] F. E. Marble and S. M. Candel. acoustic disturbance from gas non-uniformities convected through a nozzle. *Journal of Sound and Vibration*, 55:225–243, 1977.
- [18] J. E. Ffowes Williams and M S Howe. The generation of sound by density inhomogeneities in low mach number nozzle flows. *Journal of Fluid Mechanics*, 70(3):605–622, 1975.
- [19] M. Leyko, S. Moreau, F. Nicoud, and T. Poinso. Numerical and analytical modelling of entropy noise in a supersonic nozzle with a shock. *Journal of Sound and Vibration*, 330(16):3944–3958, 2011.
- [20] L. Hirschberg, S. J. Hulshoff, and F. Bake. Sound production due to swirl-nozzle interaction: Model-based analysis of experiments. *AIAA Aviation 2020 Forum*, pages 1–23, Virtual Event, June 15-19, 2020.
- [21] L. Hirschberg, S. J. Hulshoff, and F. Bake. Sound production due to swirl–nozzle interaction: Model-based analysis of experiments. *AIAA Journal*, 59(4):1269–1276, 2021.
- [22] J.-Y. Lestrade, J. Anthoine, A.J. Musker, and A. Lecossais. Experimental demonstration of an end-burning swirling flow hybrid rocket engine. *Aerospace Science and Technology*, 92:1–8, 2019.
- [23] Gaurav Sharma and Joseph Majdalani. Effects of nozzle inlet size and curvature on the flow development in a bidirectional vortex chamber. *Physics of Fluids*, 33(9):093607, 2021.
- [24] D. Neuhaus and I. Röhle. Schnellschaltende ventile für anwendungen in der luft und raumfahrt. In *Deutscher Luft- und Raumfahrtkongress*, 2006.
- [25] L. Hirschberg, F. Bake, K. Knobloch, Hulshoff S. J., and Hirschberg A. Experimental investigations of indirect noise due to modulation of axial vorticity and entropy upstream of a choked nozzle. *Journal of Sound and Vibration*, under review, 2022.
- [26] P. A. Thompson. *Compressible-Fluid Dynamics*. MacGraw Hill, NY, USA, 1972.